surfaces

MDPI

Article

Adsorption of Gadolinium Bisphthalocyanine on Atomically Flat Surfaces: Comparison of Graphene and Hexagonal Boron Nitride from DFT Calculations

Vladimir A. Basiuk [1,*] and Elena V. Basiuk [2]

[1] Instituto de Ciencias Nucleares, Universidad Nacional Autónoma de México, Circuito Exterior C.U., Ciudad de México 04510, Mexico
[2] Instituto de Ciencias Aplicadas y Tecnología, Universidad Nacional Autónoma de México, Circuito Exterior C.U., Ciudad de México 04510, Mexico; elena.golovataya@icat.unam.mx
* Correspondence: basiuk@nucleares.unam.mx

Abstract: We studied the noncovalent interactions of gadolinium bisphthalocyanine ($GdPc_2$) with cluster models for graphene and hexagonal boron nitride (*h*BN) of variable size by using the PBE functional of the generalized gradient approximation in conjunction with Grimme's dispersion correction and a DND double numerical basis set (that is, PBE-D2/DND). We found that in terms of the bonding strength, changes in the Gd-N bond lengths, the charge and spin of the Gd central ion, and the spin of the $GdPc_2$ molecule, the behaviors of the graphene- and *h*BN-based model systems are rather similar. As expected, when increasing the size of the graphene and *h*BN cluster models, the strength of the interaction with $GdPc_2$ increases, in which the bonding with the *h*BN models is usually stronger by a few kcal/mol. One of the main questions addressed in the present work was whether a change in the antiferromagnetic spin alignment to a ferromagnetic one, which is typical for $GdPc_2$, is (at least theoretically) possible, as it has been observed previously for a number of graphene models when a smaller basis set DN was employed. We found that the use of a larger DND basis set dramatically reduces the occurrence of ferromagnetic adsorption complexes but does not exclude this possibility completely.

Keywords: gadolinium bisphthalocyanine; adsorption; graphene; hexagonal boron nitride; DFT calculations

Citation: Basiuk, V.A.; Basiuk, E.V. Adsorption of Gadolinium Bisphthalocyanine on Atomically Flat Surfaces: Comparison of Graphene and Hexagonal Boron Nitride from DFT Calculations. *Surfaces* **2024**, *7*, 404–413. https://doi.org/10.3390/surfaces7020025

Academic Editor: Gaetano Granozzi

Received: 10 April 2024
Revised: 14 May 2024
Accepted: 29 May 2024
Published: 1 June 2024

1. Introduction

The deposition of single-molecule magnets (SMMs) onto solid surfaces and nanomaterials is considered as an essential step for their application in spintronic devices (see, for example, [1–10]). A special emphasis is placed on graphene (per se, or an upper layer of highly oriented pyrolytic graphite, HOPG) as a solid support [1–10] as well as on lanthanide bisphthalocyanines ($LnPc_2$, where Ln = Tb, Dy, Er) as representative SMMs [1–6,8–10].

The popularity of graphene, which is considered one of the most crucial and promising nanomaterials, needs no additional comments or justifications. A rather curious observation in the present context of surface-deposited SMMs is that its 'sibling', hexagonal boron nitride (*h*BN) [11], has received much less attention. This is exemplified by the study of manganese-containing dimers (with ligands other than Pcs) on graphene and *h*BN [7] and the study [12] in which $TbPc_2$ deposited onto *h*BN was considered very briefly, for the sake of comparison with MgO-supported bisphthalocyanine.

The interest in $TbPc_2$- and $DyPc_2$-containing systems is quite understandable due to their very complex magnetic behaviors, with very high calculated and experimental magnetic moments [13]. At the same time, their gadolinium analogue $GdPc_2$ [13–16] deserves attention as well. Formally, it has the highest (of the entire $LnPc_2$ family) number of unpaired electrons: seven on the half-filled 4*f* shell, plus one π-electron delocalized on

the two Pc ligands. However, as a result of strong antiferromagnetic coupling, when the 4*f* electrons and the π-electron have opposite directions, instead of the theoretical magnetic moment of 7.94 BM, this value decreases to 6.9 BM [13,15].

Experimental measurements are of primary importance in the area of SMMs deposited onto solid supports, but only limited research has been undertaken to complement these with theoretical results [2,4,7]. The latter fact is easily explainable, since, as Marocchi et al. [4] fairly noted, "simulating rare earths within DFT is very tricky, due to the strong electronic correlation effects in 4*f*-electrons". We learned this through our own experience when we attempted to study by means of the density functional theory (DFT) the full series (from La to Lu) of lanthanide-containing molecules, such as $LnPc_2$ bisphthalocyanines [17], endohedral fullerenes $Ln@C_{60}$ [18] and $Ln_3N@I_h$-C_{80} [19], as well as lanthanide atoms and ions interacting with both cluster [20,21] and periodic [22] graphene models. Nevertheless, along with the serious (sometimes unresolvable) problems of self-consistent field (SCF) convergence for the Tb- and Dy-containing systems, we found that the case of their closest neighbor Gd might be as simple as the cases of La (with a totally empty 4*f* shell) and Lu (with a completely filled 4*f* shell), due to the half-filled 4*f* shell and zero orbital moment. This property allowed us to successfully perform calculations for $GdPc_2$ adsorbed on carbon nanotube [23] and graphene (both pristine and defect-containing) models [24].

In both works [23,24], we focused mostly on the variations in the geometry and interaction strength of $GdPc_2$ with different carbon nanoclusters. At the same time, perhaps the most interesting (from our point of view) result is related to the spin coupling (or alignment) pattern. It was antiferromagnetic only in a limited number of calculations, similar to isolated $GdPc_2$ [13,15,17] with an absolute value for its molecular spin of 6.007*e* [24], whereas for most adsorption complexes (including those with all graphene models), the coupling became ferromagnetic, reaching absolute spin values of almost 8*e* [24].

This latter observation served as the foundation for the present study. The previous calculations [24] employed the double-numerical basis set DN, without polarization functions added to any atoms, and thus, the ferromagnetic coupling might have been simply a small basis set-related artifact. In the present work, we added a polarization function to all non-hydrogen atoms (that is, we used a DND basis set) to eliminate this possibility. Our second goal was to compare the behavior of graphene and its 'sibling' *h*BN, in terms of the bonding strength, changes in Gd-N bond lengths, the charge and spin of the Gd central ion, as well as the spin of the $GdPc_2$ molecule. And our third goal was to trace how all the above characteristics change when varying the size of the graphene and *h*BN cluster model. In this way, we attempted to provide new detailed information to the obviously underexplored area of $LnPc_2$ interactions with nanomaterials such as graphene and especially *h*BN.

2. Methods

A theoretical analysis of bonding strength, geometries, and electronic parameters of noncovalent complexes of $GdPc_2$ with graphene and *h*BN cluster models of variable size was performed by employing the numerical-based DFT module $DMol^3$ of the Materials Studio suite [25–28]. As in all previous related works mentioned above [17–24], the PBE (by Perdew-Burke-Ernzerhof [29]) general gradient approximation function was used in conjunction with the empirical dispersion correction introduced by Grimme [30], that is, the PBE-D2 combination. (One should note that for noncovalent complexes of tetraazaannulenes with carbon nanoclusters, PBE-D2 yields more realistic geometries than, for example, the widely used hybrid functional B3LYP [31].)

As already mentioned in the introduction, the size of the double-numerical basis set (DN in [23,24]) was increased by adding a polarization *d*-function to all non-H atoms, that is, to DND (which is equivalent to the 6-31G(d) Pople-type basis set). The settings employed for the full geometry optimization and the calculation of the electronic parameters included the use of DFT semi-core pseudopotentials (DSPPs) and a real space (or orbital) cutoff of 5.0 Å, as dictated by the presence of gadolinium atoms. The convergence criteria were as follows: an energy gradient of 2×10^{-5} Ha, maximum force of 0.004 Ha/Å, maximum

displacement of 0.005 Å, and SCF tolerance of 10^{-5} Ha. A special comment has to be added about the use of thermal smearing to facilitate SCF convergence. In the present calculations, we followed the general protocol explained in detail in earlier studies [32–34]. In principle, it was found that the use of a very low value of 0.0001 Ha (equivalent temperature of 31.6 K) yields stable and consistent results, which are essentially identical to those afforded by applying Fermi occupancy (that is, zero smearing). Consequently, we usually set 0.0001 Ha as the target value to elaborate on final publishable results [17–24]. While for the derivatives of Tb and some other lanthanides, this value does not allow to achieve SCF convergence and has to be increased, the Gd-containing systems (like the ones incorporating La and Lu atoms) often can be successfully treated at the Fermi occupancy. We took advantage of this possibility in the present paper.

We would like to mention one of the differences in functioning between Gaussian and DMol^3 software, which is especially important in the present context of quantum chemical calculations of lanthanide-containing systems. While in the Gaussian software, a total spin of the system has to be assigned in the input (see, for example, references [15,35–37]), and it is also possible to specify a particular spin value in DMol^3, the option we employed for all calculations was "Use formal spin as initial". That is, the calculations were unconstrained.

The formation energies $\Delta E_{\mathrm{GdPc2+S}}$ (or simply ΔE) were calculated by using the following general equation:

$$\Delta E_{\mathrm{GdPc2+S}} = E_{\mathrm{GdPc2+S}} - (E_{\mathrm{GdPc2}} + E_{\mathrm{S}})$$

where E_i is the respective absolute energy, and S is surface model.

3. Results and Discussion

The cluster models we tested for graphene and *h*BN, as well as the typical optimized geometry (staggered conformation) for $GdPc_2$, are shown in Figure 1. All the models simulating graphene and *h*BN are hexagonal. The smallest ones are benzene (C_6H_6) and borazine ($B_3N_3H_6$), respectively, in which each side of the hexagon has one H atom. (Strictly speaking, these molecules may not adequately capture the electronic properties of the extended sheets; they were included simply for the completeness of both series.) Using a uniform and easily understood nomenclature, they are denoted as C-1H and BN-1H, respectively. In a similar way, coronene and its BN analogue are referred to as C-2H and BN-2H, respectively; supercoronene and its BN analogue are referred to as C-3H and BN-3H, respectively, and so on. The largest members of the two series are C-7H and BN-7H. Also, within the carbon-based models, we included fullerene C_{60}, for comparison: the planar model closest to this fullerene (in terms of molecular weight) is C-3H, with the chemical formula $C_{54}H_{18}$. The latter model has a slightly smaller diagonal span (about 14.4 Å) compared to that of $GdPc_2$ (15.2 Å), and the larger graphene models start with C-4H (19.3 Å). In the case of the *h*BN models BN-3H and BN-4H, the measurements are similar, 14.7 and 19.7 Å, respectively, despite the differences in the bond lengths of C–C and C–H versus B–N, B–H, and N–H. In other words, only starting from C-4H and BN-4H, $GdPc_2$ can fully fit onto the model surface.

Both components undergo a bending distortion, as a result of strong π–π stacking interactions: this is exemplified for the $GdPc_2$ + C-6H and $GdPc_2$ + BN-6H complexes in Figure 2. The surface model tends to 'embrace' the $GdPc_2$ molecule, which is more evident here for the latter complex. In turn, the "lower" Pc ligand (the one in contact with the surface) becomes more planar for the same reason, whereas the opposite one (denoted as the "upper" one) does not exhibit visible changes, as compared to the Pc ligands in the isolated bisphthalocyanine.

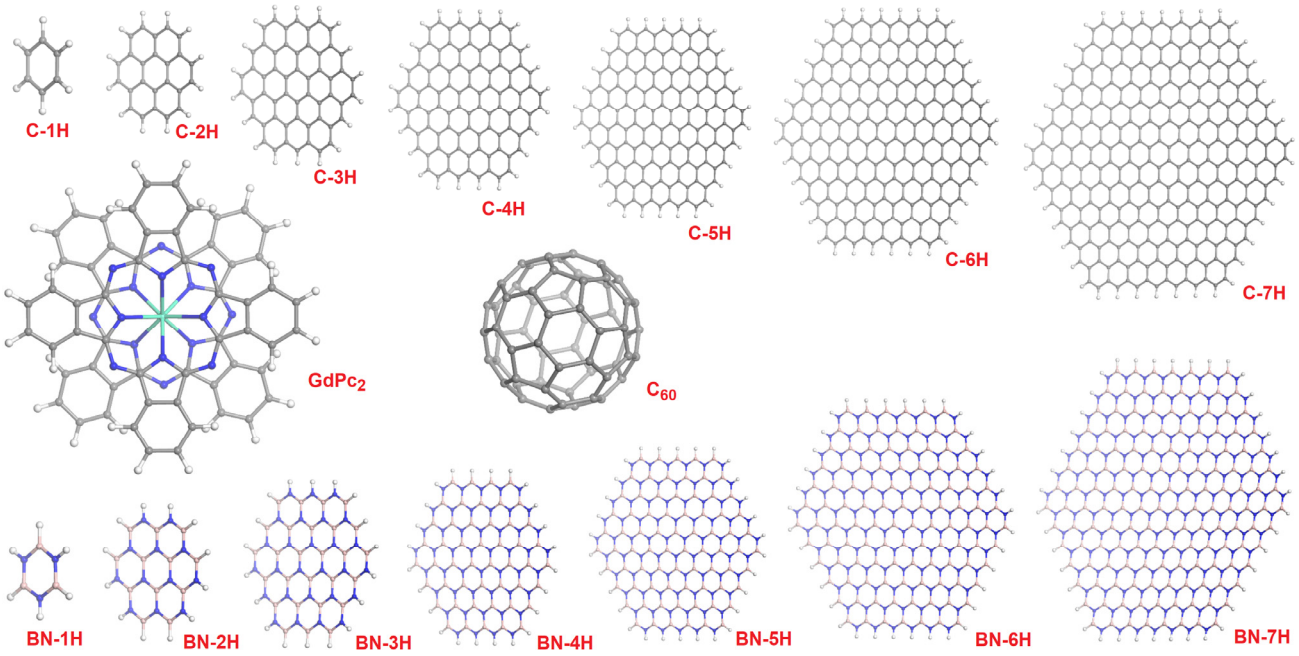

Figure 1. The models employed in our cluster calculations. Atom colors: grey, carbon; white, hydrogen; deep blue, nitrogen; pink, boron; light blue green, gadolinium.

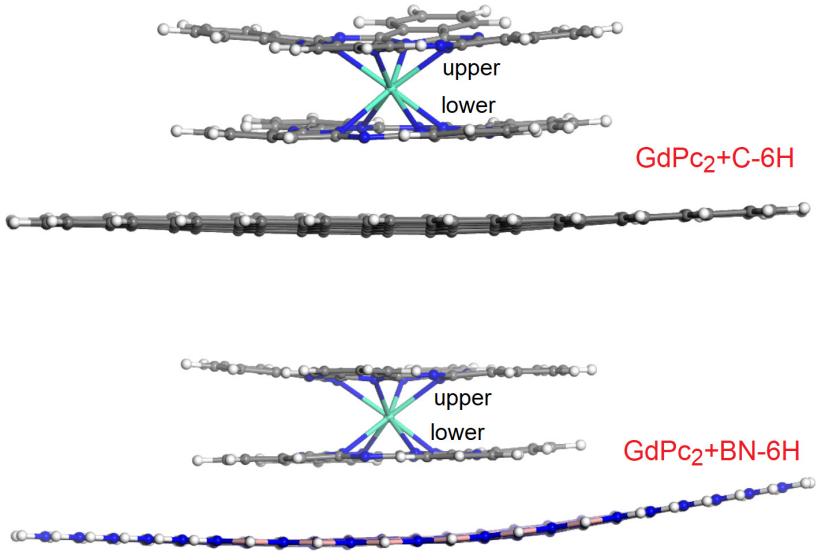

Figure 2. Representative geometries of $GdPc_2$ + C-nH and $GdPc_2$ + BN-nH complexes (exemplified for n = 6, that is, C-6H and BN-6H in Figure 1). Pc ligands are denoted as "upper" or "lower".

Among the central questions we addressed is that of the comparative strengths of the $GdPc_2$ interactions for the graphene and *h*BN models. The numerical results for the corresponding ΔE bonding energies are presented in Table 1, as well as in graphical form in Figure 3a.

Table 1. Total energies (E) for all isolated components and the corresponding noncovalent complexes, formation energies (ΔE) for noncovalent complexes of $GdPc_2$ with carbon- and boron nitride-based models, average Gd-N bond lengths, as well as charge and spin of Gd ion, along with the total spin of $GdPc_2$ molecule, obtained from the Mulliken population analysis.

	E_{total} (Ha)	ΔE (kcal/mol)	Gd-N_{lower} (Å) [a]	Gd-N_{upper} (Å)	Gd Charge (e)	Gd Spin (e)	$GdPc_2$ Spin (e)
$GdPc_2$	−3528.7468834		2.450	2.450	1.300	7.007	6.011
C-1H	−232.0208765						
C-2H	−921.0808194						
C-3H	−2067.1815845						
C-4H	−3670.3260780						
C-5H	−5730.5170328						
C-6H	−8247.7564282						
C-7H	−11,222.0439594						
C_{60}	−2284.4334844						
BN-1H	−242.4167720						
BN-2H	−962.7988404						
BN-3H	−2161.1563381						
BN-4H	−3837.4911698						
BN-5H	−5991.8039867						
BN-6H	−8624.0947660						
BN-7H	−11,734.3621054						
$GdPc_2$ + C-1H	−3760.7904162	−14.2	2.447	2.453	1.367	−7.006	−6.010
$GdPc_2$ + C-2H	−4449.8723439	−28.0	2.487	2.473	1.364	−7.000	−6.096
$GdPc_2$ + C-3H	−5596.0080928	−50.0	2.429	2.439	1.344	7.005	6.038
$GdPc_2$ + C-4H	−7199.1737356	−63.2	2.439	2.426	1.353	−7.004	−6.065
$GdPc_2$ + C-5H	−9259.3781214	−71.7	2.427	2.445	1.324	7.004	6.041
$GdPc_2$ + C-6H	−11,776.6182309	−72.1	2.420	2.420	1.307	−7.002	−7.974
$GdPc_2$ + C-7H	−14,750.9094551	−74.4	2.429	2.446	1.320	7.004	6.034
$GdPc_2$ + C_{60}	−5813.2211513	−25.6	2.424	2.440	1.333	7.008	6.014
$GdPc_2$ + BN-1H	−3771.1790578	−9.7	2.492	2.493	1.408	7.003	6.008
$GdPc_2$ + BN-2H	−4491.6012679	−34.9	2.452	2.462	1.350	7.002	6.020
$GdPc_2$ + BN-3H	−5689.9869344	−52.5	2.443	2.427	1.328	7.005	6.019
$GdPc_2$ + BN-4H	−7366.3531079	−72.2	2.467	2.432	1.335	−7.004	−6.028
$GdPc_2$ + BN-5H	−9520.6731475	−76.7	2.429	2.424	1.316	−7.005	−6.019
$GdPc_2$ + BN-6H	−12,152.9688187	−79.8	2.415	2.433	1.307	−7.002	−7.982
$GdPc_2$ + BN-7H	−15,263.2324587	−77.5	2.434	2.410	1.303	−7.007	−6.024
$(GdPc_2)_2$	−7057.5896494	−60.2	2.427	2.429	1.337, 1.337	7.004, −7.004	7.006, −7.004

[a] Lower, indicating Pc ligand is in contact with the surface in carbon- and boron nitride-based model; upper, for opposite Pc ligand (Figure 2). Equivalent for isolated $GdPc_2$.

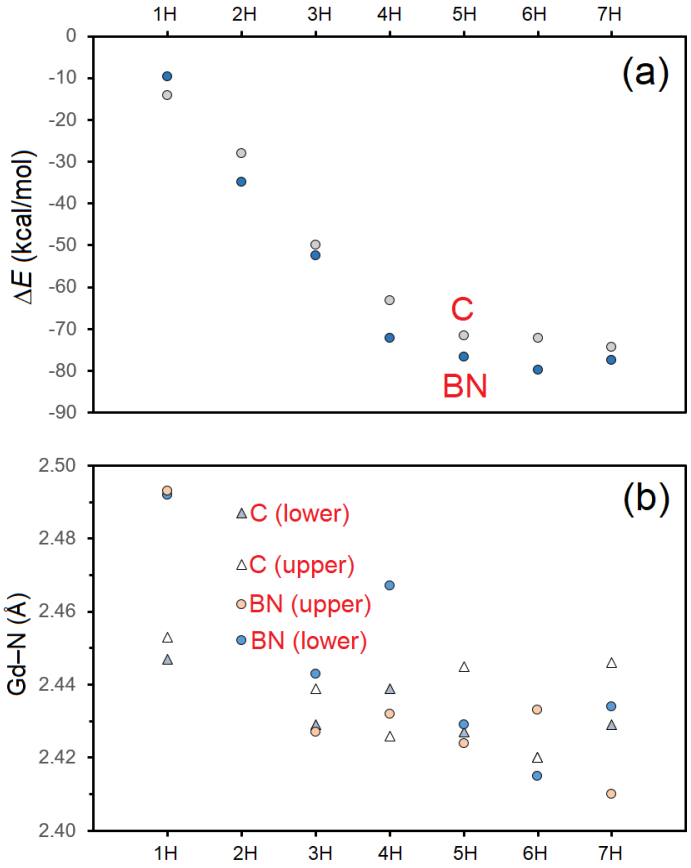

Figure 3. Graphical representation of the changes in the energy of complex formation (**a**) and the average Gd-N distance (**b**) depending on the size of C-nH and BN-nH cluster model. The case of C_{60} is not included.

In the case of the graphene models, the weakest interaction, of −14.2 kcal/mol, was logically found with the benzene molecule (the smallest C-1H model), reaching −74.4 kcal/mol for the largest nanocluster C-7H. Despite the fact that the molecular weight of C_{60} fullerene best matches that of the C-3H model, its strong spherical curvature prevents efficient contact between the two components, and the Δ*E* value of −25.6 kcal/mol for $GdPc_2$ + C_{60} is actually closer to the one of −28.0 kcal/mol obtained for $GdPc_2$ + C-2H. With the exception of the first member of the *h*BN models, that is, borazine (Δ*E* of −9.7 kcal/mol), their bonding with $GdPc_2$ is stronger compared to that of the analogous graphene models, roughly by a few kcal/mol. From Figure 3a, it is more evident that until reaching the complexes with C-4H and BN-4H, the Δ*E* values tend to decrease almost linearly, then the changes become less apparent. While the lowest Δ*E* value in the carbon series was obtained for the largest nanocluster C-7H, in the case of the BN series, the bonding strength slightly fluctuates: −76.7, −79.8, and −77.5 kcal/mol for $GdPc_2$ + BN-5H, $GdPc_2$ + BN-6H, and $GdPc_2$ + BN-7H, respectively. That is, the strongest bonding was obtained with the BN-6H model. For comparison, we also calculated the formation energy for the $(GdPc_2)_2$ π–π stacking dimer, which is −60.2 kcal/mol, and thus is situated between those obtained for the $GdPc_2$ + X-3H and $GdPc_2$ + X-4H (X = C, BN) noncovalent complexes.

The changes in $GdPc_2$ geometry were estimated in terms of average Gd-N distances, both in the "lower" and in the "upper" phthalocyanine coordination spheres (Table 1 and Figure 3b). In the case of the isolated $GdPc_2$ molecule, their values are equal to 2.450 Å. As a result of the flattening of the "lower" Pc unit, one might expect some shortening of Gd-N coordination bonds compared to the ones found in the "upper" phthalocyanine part. Nevertheless, no such trend can be observed; in some cases, the "lower" Gd-N distances indeed become shorter (the largest difference of 0.018 Å was found in the $GdPc_2$ + C-5H and

$GdPc_2$ + BN-6H complexes), in others, they increase (by up to 0.035 Å in $GdPc_2$ + BN-4H). As a whole, from Figure 3b, one can conclude that the shorter Gd-N coordination bonds are associated with the larger graphene and *h*BN models. However, when considering each of the four series of the Gd-N distances separately, the changes become rather random, without any clear tendency.

One of the electronic parameters analyzed was the (positive) charge of the Gd ion (Table 1). In the isolated $GdPc_2$ molecule, it is 1.300*e*, with a notable increase to 1.337*e* on both gadolinium ions in the $(GdPc_2)_2$ dimer. Similarly, it increases upon complexation with any graphene or *h*BN model. In the latter case, the span of Gd charge values is especially wide, from a very minor increase to 1.303*e* in $GdPc_2$ + BN-7H to a rather high value of 1.408*e* for the first member of the BN series, $GdPc_2$ + BN-1H. In the graphene series, the corresponding values are found to be between 1.307 e ($GdPc_2$ + C-6H) and 1.367*e* ($GdPc_2$ + C-1H). At the same time, the spin of the Gd ion is a relatively invariant characteristic, though its direction (up and down, meaning positive and negative values, respectively) is random. In the isolated $GdPc_2$ molecule, it is 7.007*e* (spin-up, as shown in Figure 4). In the $(GdPc_2)_2$ dimer, both absolute Gd spin values are the same of 7.004*e*, but with opposite signs/directions (Table 1). The lowest absolute value of 7.000*e* was obtained for the $GdPc_2$ + C-2H complex, and the highest one of 7.008*e* was obtained for the fullerene derivative $GdPc_2$ + C_{60}.

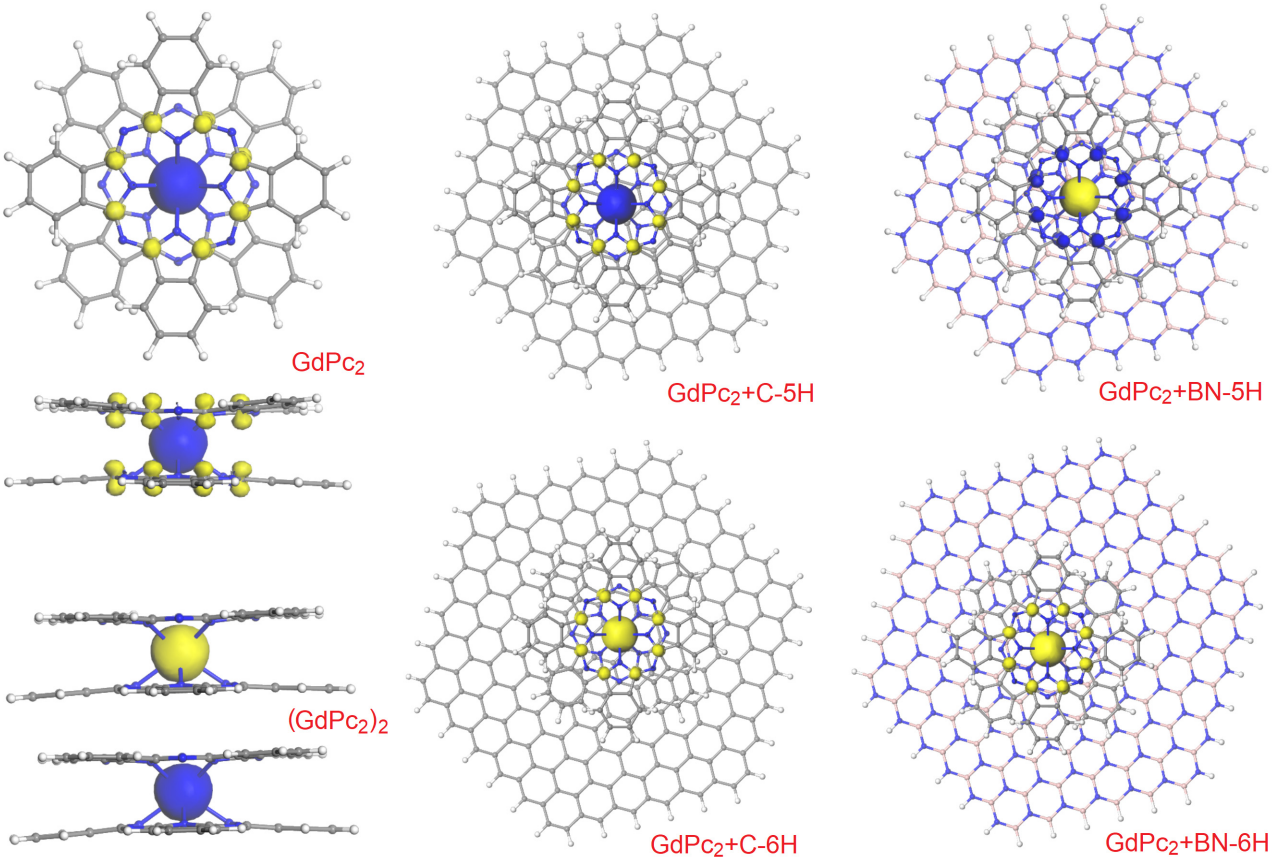

Figure 4. Different observed patterns of spin density distribution (isosurfaces at 0.02 a.u.) exemplified by isolated $GdPc_2$, noncovalent dimer $(GdPc_2)_2$, and $GdPc_2$ adsorption complexes with C-5H, C-6H, BN-5H, and BN-6H models. Lobe colors: blue, spin-up electrons; yellow, spin-down electrons.

Now, the most interesting question is related to the possibility of ferromagnetic spin alignment within the $GdPc_2$ molecule. As was mentioned in the introduction, it was antiferromagnetic only in a limited number of the previous calculations with defect-free and defect-containing graphene models, such as in isolated $GdPc_2$, whereas for most adsorption

complexes, the coupling became ferromagnetic, reaching absolute spin values of almost 8*e* [24]. But the previous [24] and the present study employed the double-numerical basis sets of different sizes: DN (with no polarization functions for any atoms) and DND (with a polarization function on all non-H atoms), respectively: the use of the DND basis set is supposed to yield a more realistic picture. All the numerical data obtained are summarized in Table 1, and the most representative spin density plots are shown in Figure 4. The molecular spin of the isolated $GdPc_2$ molecule, as computed with the DND basis set, is 6.011*e* due to the antiferromagnetic coupling typical for this and some other lanthanide bisphthalocyanines [13,15,17], in which the 4*f* electrons of the Gd ion and the π-electron have opposite directions (Figure 4). As it could be expected, in the system composed of two $GdPc_2$ molecules (that is, the $(GdPc_2)_2$ dimer), the two π-electrons become paired, and no spin density lobes are observed on phthalocyanine ligands; on the other hand, nothing like this can happen to the 4*f* electrons of the two Gd ions. As a result, the absolute values of the spins of the two $GdPc_2$ molecules are defined by the spins of their Gd ions, which are essentially equal but have opposite signs (7.006 and −7.004*e*).

In the case of the $GdPc_2$ interacting with the graphene and *h*BN models, the situation observed previously [24], in which the DN basis set was used, changes quantitatively, but not qualitatively. Now, the dominating pattern of the spin alignment is antiferromagnetic, as in the isolated $GdPc_2$ molecule; this is exemplified in Figure 4 for the $GdPc_2$ + C-5H and $GdPc_2$ + BN-5H complexes. The spin directions (spin-up and spin-down) of the the 4*f* electrons of the Gd ion and the π-electron of Pc can invert, which does not imply any changes in properties in the absence of an external field. We obtained a ferromagnetic alignment in only two complexes, $GdPc_2$ + C-6H and $GdPc_2$ + BN-6H, though we cannot offer an explanation why this was observed specifically for C-6H and BN-6H, but not for smaller or larger models. The corresponding $GdPc_2$ molecular spins are −7.974*e* and −7.982*e* (all the electrons are spin-down); that is, their absolute values almost reach 8*e* [24]. For all of the remaining antiferromagnetic cases, the absolute values of the $GdPc_2$ molecular spin fluctuate insignificantly: for the graphene models, between 6.010*e* ($GdPc_2$ + C-1H) and 6.096*e* ($GdPc_2$ + C-2H) and for *h*BN models, between 6.008*e* ($GdPc_2$ + BN-1H) and 6.028*e* ($GdPc_2$ + BN-4H). In other words, no spin transfer is observed from the $GdPc_2$ to the surface model, and no spin density lobes can be detected on the latter in the spin density plots (Figure 4).

4. Conclusions

In terms of the bonding strength, changes in the Gd-N bond lengths, the charge and spin of the Gd central ion, and the spin of the $GdPc_2$ molecule, the behaviors of graphene- and *h*BN-based model systems are rather similar. When increasing the size of the graphene and *h*BN cluster models, the strength of interactions with $GdPc_2$ naturally increases, and the bonding with the *h*BN model is usually stronger by a few kcal/mol.

One of the main questions addressed in the present work was whether the change in antiferromagnetic spin alignment, which is typical for gadolinium bisphthalocyanine, to a ferromagnetic one is (at least theoretically) possible or it is just an artifact associated with a smaller basis set DN (equivalent to 6-31G) [24]. In this regard, we found that the use of the larger DND basis set dramatically reduces the occurrence of ferromagnetic adsorption complexes, but does not exclude this possibility completely. It would be highly desirable to have an explanation for why these changes occur specifically with certain cluster sizes or structures. Unfortunately, one of the necessary steps this entails would be to explore a much broader variety of graphene and *h*BN models, for example, in terms of nanocluster size and geometry. However, this would entail increased computational cost and effort, which goes beyond our capabilities at present.

Author Contributions: Conceptualization, V.A.B. and E.V.B.; methodology, V.A.B. and E.V.B.; formal analysis, V.A.B. and E.V.B.; resources, V.A.B.; data curation, V.A.B. and E.V.B.; writing—original draft preparation, V.A.B.; writing—review and editing, V.A.B. and E.V.B.; visualization, V.A.B. and E.V.B.;

supervision, V.A.B.; project administration, V.A.B.; funding acquisition, V.A.B. All authors have read and agreed to the published version of the manuscript.

Funding: This research was funded by the National Autonomous University of Mexico (UNAM), grant DGAPA-IN103622, project title "Efectos topológicos en las interacciones de las especies de "tierras raras" con nanomateriales de carbono de baja dimensionalidad".

Institutional Review Board Statement: Not applicable.

Informed Consent Statement: Not applicable.

Data Availability Statement: The data presented in this study are available upon request from the corresponding author.

Conflicts of Interest: The authors declare no conflicts of interest.

References

1. Candini, A.; Klyatskaya, S.; Ruben, M.; Wernsdorfer, W.; Affronte, M. Graphene spintronic devices with molecular nanomagnets. *Nano Lett.* **2011**, *11*, 2634–2639. [CrossRef] [PubMed]
2. Gonidec, M.; Biagi, R.; Corradini, V.; Moro, F.; De Renzi, V.; del Pennino, U.; Summa, D.; Muccioli, L.; Zannoni, C.; Amabilino, D.B.; et al. Surface supramolecular organization of a terbium(III) double-decker complex on graphite and its single molecule magnet behavior. *J. Am. Chem. Soc.* **2011**, *133*, 6603–6612. [CrossRef] [PubMed]
3. Klar, D.; Candini, A.; Joly, L.; Klyatskaya, S.; Krumme, B.; Ohresser, P.; Kappler, J.-P.; Ruben, M.; Wende, H. Hysteretic behaviour in a vacuum deposited submonolayer of single ion magnets. *Dalton Trans.* **2014**, *43*, 10686–10689. [CrossRef] [PubMed]
4. Marocchi, S.; Candini, A.; Klar, D.; Van den Heuvel, W.; Huang, H.; Troiani, F.; Corradini, V.; Biagi, R.; De Renzi, V.; Klyatskaya, S.; et al. Relay-like exchange mechanism through a spin radical between $TbPc_2$ molecules and graphene/Ni(111) substrates. *ACS Nano* **2016**, *10*, 9353–9360. [CrossRef] [PubMed]
5. Corradini, V.; Candini, A.; Klar, D.; Biagi, R.; De Renzi, V.; Lodi Rizzini, A.; Cavani, N.; del Pennino, U.; Klyatskaya, S.; Ruben, M.; et al. Probing magnetic coupling between $LnPc_2$ (Ln = Tb, Er) molecules and the graphene/Ni(111) substrate with and without Au-intercalation: Role of the dipolar field. *Nanoscale* **2018**, *10*, 277–283. [CrossRef] [PubMed]
6. Serrano, G.; Velez-Fort, E.; Cimatti, I.; Cortigiani, B.; Malavolti, L.; Betto, D.; Ouerghi, A.; Brookes, N.B.; Mannini, M.; Sessoli, R. Magnetic bistability of a $TbPc_2$ submonolayer on a graphene/SiC(0001) conductive electrode. *Nanoscale* **2018**, *10*, 2715–2720. [CrossRef] [PubMed]
7. Berkley, R.S.; Hooshmand, Z.; Jiang, T.; Le, D.; Hebard, A.F.; Rahman, T.S. Characteristics of single-molecule magnet dimers ($[Mn_3]_2$) on graphene and *h*-BN. *J. Phys. Chem. C* **2020**, *124*, 28186–28200. [CrossRef]
8. Yin, X.; Deng, L.; Ruan, L.; Wu, Y.; Luo, F.; Qin, G.; Han, X.; Zhang, X. Recent progress for single-molecule magnets based on rare earth elements. *Materials* **2023**, *16*, 3568. [CrossRef]
9. Liu, S.; Zhu, Z.; Zhang, P.; Tang, J. Chemisorption of lanthanide single-molecule magnets on surfaces. *Fundam. Res.* **2023**. [CrossRef]
10. Gabarró-Riera, G.; Aromí, G.; Sañudo, E.C. Magnetic molecules on surfaces: SMMs and beyond. *Coord. Chem. Rev.* **2023**, *475*, 214858. [CrossRef]
11. Auwärter, W. Hexagonal boron nitride monolayers on metal supports: Versatile templates for atoms, molecules and nanostructures. *Surf. Sci. Rep.* **2019**, *74*, 1–95.
12. Wäckerlin, C.; Donati, F.; Singha, A.; Baltic, R.; Rusponi, S.; Diller, K.; Patthey, F.; Pivetta, M.; Lan, Y.; Klyatskaya, S.; et al. Giant hysteresis of single-molecule magnets adsorbed on a nonmagnetic insulator. *Adv. Mater.* **2016**, *28*, 5195–5199. [CrossRef]
13. Trojan, K.L.; Kendall, J.L.; Kepler, K.D.; Hatfield, W.E. Strong exchange coupling between the lanthanide ions and the phthalocyaninato ligand radical in bis(phthalocyaninato)lanthanide sandwich compounds. *Inorg. Chim. Acta* **1992**, *198–200*, 795–803. [CrossRef]
14. Korolev, V.V.; Lomova, T.N.; Ramazanova, A.G.; Korolev, D.V.; Mozhzhukhina, E.G. Phthalocyanine-based molecular paramagnets. Effect of double-decker structure on magnetothermal properties of gadolinium complexes. *J. Organometal. Chem.* **2016**, *819*, 209–215. [CrossRef]
15. Kratochvílová, I.; Šebera, J.; Paruzel, B.; Pfleger, J.; Toman, P.; Marešová, E.; Havlová, Š.; Hubík, P.; Buryi, M.; Vrňata, M.; et al. Electronic functionality of Gd-bisphthalocyanine: Charge carrier concentration, charge mobility, and influence of local magnetic field. *Synth. Met.* **2018**, *236*, 68–78. [CrossRef]
16. Taran, G.; Moreno-Pineda, E.; Schulze, M.; Bonet, E.; Ruben, M.; Wernsdorfer, W. Direct determination of high-order transverse ligand field parameters via μSQUID-EPR in a Et_4N [$^{160}GdPc_2$] SMM. *Nat. Commun.* **2023**, *14*, 3361. [CrossRef] [PubMed]
17. Martínez-Flores, C.; Bolivar-Pineda, L.M.; Basiuk, V.A. Lanthanide bisphthalocyanine single-molecule magnets: A DFT survey of their geometries and electronic properties from lanthanum to lutetium. *Mater. Chem. Phys.* **2022**, *287*, 126271. [CrossRef]
18. Martínez-Flores, C.; Basiuk, V.A. Ln@C_{60} endohedral fullerenes: A DFT analysis for the complete series from lanthanum to lutetium. *Comp. Theor. Chem.* **2022**, *1217*, 113878. [CrossRef]

19. Martínez-Flores, C.; Basiuk, V.A. DFT analysis of the electronic and structural properties of lanthanide nitride cluster fullerenes $Ln_3N@C_{80}$. *Inorganics* **2023**, *11*, 223. [CrossRef]
20. Basiuk, V.A.; Acevedo-Guzmán, D.A.; Meza-Laguna, V.; Álvarez-Zauco, E.; Huerta, L.; Serrano, M.; Kakazey, M.; Basiuk, E.V. High-energy ball-milling preparation and characterization of Ln_2O_3−graphite nanocomposites. *Mater. Today Commun.* **2021**, *26*, 102030. [CrossRef]
21. Basiuk, E.V.; Prezhdo, O.V.; Basiuk, V.A. Strong bending distortion of supercoronene graphene model upon adsorption of lanthanide atoms. *J. Phys. Chem. Lett.* **2023**, *14*, 2910–2916. [CrossRef] [PubMed]
22. Basiuk, V.A.; Prezhdo, O.V.; Basiuk, E.V. Adsorption of lanthanide atoms on graphene: Similar, yet different. *J. Phys. Chem. Lett.* **2022**, *13*, 6042–6047. [CrossRef] [PubMed]
23. Bolivar-Pineda, L.M.; Mendoza-Domínguez, C.U.; Basiuk, V.A. Adsorption of lanthanide double-decker phthalocyanines on single-walled carbon nanotubes: Structural changes and electronic properties as studied by density functional theory. *J. Mol. Model.* **2023**, *29*, 158. [CrossRef] [PubMed]
24. Mendoza-Domínguez, C.U.; Bolivar-Pineda, L.M.; Basiuk, V.A. Effect of structural defects in graphene on the geometry and electronic properties of adsorbed lanthanide bisphthalocyanines: A DFT analysis. *Comp. Theor. Chem.* **2023**, *1225*, 114152. [CrossRef]
25. Delley, B.; Ellis, D.E.; Freeman, A.J.; Baerends, E.J.; Post, D. Binding energy and electronic structure of small copper particles. *Phys. Rev. B* **1983**, *27*, 2132–2144. [CrossRef]
26. Delley, B. An all-electron numerical method for solving the local density functional for polyatomic molecules. *J. Chem. Phys.* **1990**, *92*, 508–517. [CrossRef]
27. Delley, B. Fast calculation of electrostatics in crystals and large molecules. *J. Phys. Chem.* **1996**, *100*, 6107–6110. [CrossRef]
28. Delley, B. From molecules to solids with the $DMol^3$ approach. *J. Chem. Phys.* **2000**, *113*, 7756–7764. [CrossRef]
29. Perdew, J.P.; Burke, K.; Ernzerhof, M. Generalized gradient approximation made simple. *Phys. Rev. Lett.* **1996**, *77*, 3865–3868. [CrossRef]
30. Grimme, S. Semiempirical GGA-type density functional constructed with a long-range dispersion correction. *J. Comput. Chem.* **2006**, *27*, 1787–1799. [CrossRef]
31. Basiuk, V.A. Interaction of tetraaza[14]annulenes with single-walled carbon nanotubes: A DFT study. *J. Phys. Chem. B* **2004**, *108*, 19990–19994. [CrossRef]
32. Michelini, M.C.; Pis Diez, R.; Jubert, A.H. A density functional study of small nickel clusters. *Int. J. Quantum Chem.* **1998**, *70*, 693–701. [CrossRef]
33. Migliore, A.; Sit, P.H.-L.; Klein, M.L. Evaluation of electronic coupling in transition-metal systems using DFT: Application to the hexa-aquo ferric−ferrous redox couple. *J. Chem. Theory Comput.* **2009**, *5*, 307–323. [CrossRef] [PubMed]
34. Basiuk, V.A.; Prezhdo, O.V.; Basiuk, E.V. Thermal smearing in DFT calculations: How small is really small? A case of La and Lu atoms adsorbed on graphene. *Mater. Today Commun.* **2020**, *25*, 101595. [CrossRef]
35. Slanina, Z.; Uhlík, F.; Akasaka, T.; Lu, X.; Adamowicz, L. Computational modeling of the $Ce@C_{82}$ metallofullerene isomeric composition. *ECS J. Solid State Sci. Technol.* **2019**, *8*, M118–M121. [CrossRef]
36. Slanina, Z.; Uhlík, F.; Akasaka, T.; Lu, X.; Adamowicz, L. Calculated relative thermodynamic stabilities of the $Gd@C_{82}$ isomers. *ECS J. Solid State Sci. Technol.* **2021**, *10*, 071013. [CrossRef]
37. Uhlík, F.; Slanina, Z.; Bao, L.; Akasaka, T.; Lu, X.; Adamowicz, L. $Eu@C_{88}$ isomers: Calculated relative populations. *ECS J. Solid State Sci. Technol.* **2022**, *11*, 101008. [CrossRef]